https://doi.org/10.2352/ISSN.2470-1173.2021.17.AVM-211

Radiometry and Photometry for Autonomous Vehicles and Machines - Fundamental Performance Limits

Robin Jenkin and Cheng Zhao; NVIDIA Corporation; Santa Clara, California, USA

Abstract

As autonomous vehicles and machines, such as self-driving cars, agricultural drones and industrial robots, become ubiquitous, there is an increasing need to understand the objective performance of cameras to support these functions. Images go beyond aesthetic and subjective roles as they assume increasing aspects of control, safety, and diagnostic capabilities. Radiometry and photometry are fundamental to describing the behavior of light and modeling the signal chain for imaging systems, and as such, are crucial for establishing objective behavior.

As an engineer or scientist, having an intuitive feel for the magnitude of units and the physical behavior of components or systems in any field improves development capabilities and guards against rudimentary errors. Back-of-the-envelope estimations provide comparisons against which detailed calculations may be tested and will urge a developer to "try again" if the order of magnitude is off for example. They also provide a quick check for the feasibility of ideas, a "giggle" or "straight-face" test as it is sometimes known.

This paper is a response to the observation of the authors that, amongst participants that are newly relying on the imaging field and existing image scientists alike, there is a general deficit of intuition around the units and order of magnitude of signals in typical cameras for autonomous vehicles and the conditions within which they operate. Further, there persists a number of misconceptions regarding general radiometric and photometric behavior. Confusion between the inverse square law as applied to illumination and consistency of image luminance versus distance is a common example.

The authors detail radiometric and photometric model for an imaging system, using it to clarify vocabulary, units and behaviors. The model is then used to estimate the number of quanta expected in pixels for typical imaging systems for each of the patches of a MacBeth color checker under a wide variety of illumination conditions. These results form the basis to establish the fundamental limits of performance for passive camera systems based both solely on camera geometry and additionally considering typical quantum efficiencies available presently. Further a mental model is given which will quickly allow user to estimate numbers of photoelectrons in pixel.

Introduction

For imaging scientists and camera engineers, anyone working with images as an input to a neural network or computer vision algorithm, or producing simulations with which to train these algorithms, light and its subsequent detection, fundamentally bound the space of engineering solutions to which we have access to. It dictates how many photons can illuminate a surface from a source and consequently the upper bound on the number that could be captured by an imaging system. In combination with imaging system parameters, it absolutely dictates the signal-to-noise ratio an image may have. And while we may apply image processing to improve the appearance of images, it is not possible to add information after the capture stage.

Given how fundamental the behavior of light and cameras are to the profession, there appears to be a number of areas of confusion between the behavior of light and imaging coupled with a general fear of radiometry and photometry. As examples, the authors have heard the comment that "[Images of] lights get darker the further from a camera they are." as a misinterpretation of the inverse square law. Also measuring "lux at the camera" rather than at the target being imaged. Finally, an observation that there is a general lack of intuition for the magnitudes of signals for typical imaging systems in the autonomous vehicle and machines field.

There are a number of excellent texts that deal with radiometry and photometry in detail, such as that by Boyd[1]. While the topic cannot be covered in great depth within this paper, a basic understanding of radiometry and photometry can be outlined in this primer with intentional simplified nomenclature and give readers tools with which to elucidate a first-order model of a source, target and camera for typical automotive systems. The model may be then used to estimate the number of quanta expected in pixels for various imaging systems for each of the patches of a MacBeth color checker and typical automotive lights under a wide variety of illumination conditions. These results form the basis to establish the fundamental limits of performance for passive camera systems based both solely on camera geometry and additionally considering typical quantum efficiencies and noise performance available presently.

The uncertainty surrounding radiometry and photometry can be summed up in one question which we will answer later in the paper. Figure 1(a), depicts a relatively straightforward scenario. Under clear weather and 10 lux ambient daylight, we are tasked with estimating the number of photoelectrons gathered in a 2.1um pixel from a car that has 20% reflective paint (Patch 22 from a MacBeth Color Checker), 100 meters from the camera. The camera has an f1.4 lens with perfect transmission. The sensor has perfect quantum efficiency between 400 and 700nm and is exposed for 10 ms. Figure 1(b) depicts the same scenario expect that the car is at 200m instead of 100m. Without reaching for a calculator or a text book, the authors challenge the reader to estimate the correct number (or even magnitude) of photoelectrons gathered by the pixel for both scenarios. Do you feel at a lost to answer this? Or do you have an idea of how to go about it but feel an urge to reach for that calculator? By the end of the paper you will be able to estimate this without a calculator. Some basic knowledge of light, lenses and imaging sensors is assumed.

Photometry and Radiometry

Photometry and radiometry both describe the measurement of the electromagnetic radiation. Radiometry may be applied to the entire electromagnetic spectrum regardless of whether it is seen or not by the eye and encompasses wavelengths from far below 0.01μm to in excess of 1000μm.

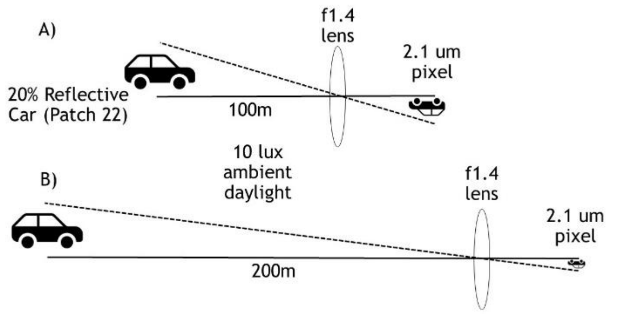

Figure 1(a) and (b). A 20% reflective car is imaged in clear weather with an exposure time of 10ms, in 10 lux ambient light with an f1.4 lens. The lens has no transmission loss and the quantum efficiency of the sensor is perfect. How many photoelectrons are generated in a 2.1μm pixel at 100m and 200m?

Photometry examines light that is perceived by the human eyes. Therefore, measurements are restricted to those wavelengths that are visible for the average human eye, about 0.36μm to 0.76μm by scaling spectral measurements with curves that describe the relative response of the eye at each wavelength, the luminous efficacy or V(λ) curve, Figure 2 [2, p39]. As may be seen, under daylight or photopic conditions, V(λ) peaks at 555nm. The peak shifts to 507nm under scotopic or dark conditions due to adaption of the eye and the reliance on rods, rather than cones to perform imaging.

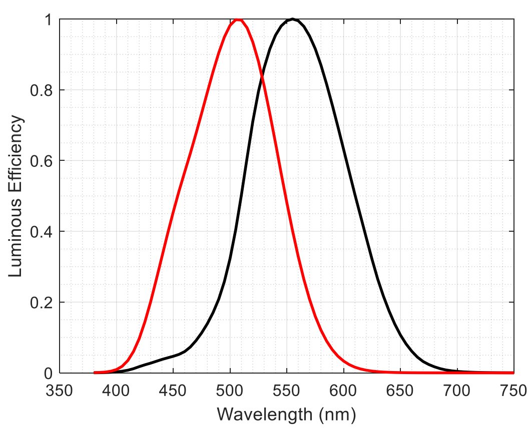

Figure 2. Spectral luminous efficiency functions under photopic (in black) and scotopic (in red) visions [2, p39].

Therefore, two parallel systems of quantities were developed for radiometry and photometry in the International Systems of Units (SI units). Radiometric measurements and units yielding results that are scaled in purely physical dimensions, such as Watts, and photometric measurements yielding units that also have physical meaning, but are scaled to account for the human eye, such as lumens. For every radiometric unit there is an equivalent photometric unit. Some of the more commonly used units are detailed below.

Due to the above, radiometry and photometry are generally applied in different applications. Radiometry is often used in areas where information concerning the absolute energy of the light is required such as astronomy, solar energy, lasers, and optoelectronics etc. Also, for applications working with wavelengths beyond the visible range, such as night vision, body and eyeball tracking, or LiDARs operating with IR light sources. Photometry is applied in the areas where light perception is the main concern such as lighting, colorimetry, and display technology. It is especially important to note that wavelengths of light beyond the perception of the human eye can still cause great damage to it and therefore radiometric calculations are more appropriate for eye safety.

Point Sources

Radiant flux (Φ), also referred as power, is radiant energy transferred per unit time. In Figure 3, radiant flux of the light source, the bulb, which we imagine to be a point source, is the total energy that is radiated from the bulb into all directions (the yellow halo surround) per second. The SI unit of radiant flux is the Watt which is equivalent to joules per second (J/s).

A portion of the energy emitted by the bulb may be intercepted by the area A. As the bulb emits equally in all directions, if we can calculate the proportion of the area of the surface of the sphere upon which area A lies, we may calculate the radiant flux that it will receive. In a similar manner that an angle defines a section of a circle in two dimensions, a solid angle defines a section of a sphere and is given the unit steradians (sr). The solid angle, **Ω**, subtended by an area, A is calculated using,

$$\Omega = \frac{A}{r^2} \tag{1}$$

where r is the radius of the circle. Similarly to a circle having 360 degrees, a sphere has a total of 4π steradians. Given the distance between the bulb and the surface, the area of the surface and the radiant flux of the source, Φ_B, we can now calculate the energy, Φ_A, received by A,

$$\Phi_A = \frac{\Phi_B \Omega}{4\pi}. \tag{2}$$

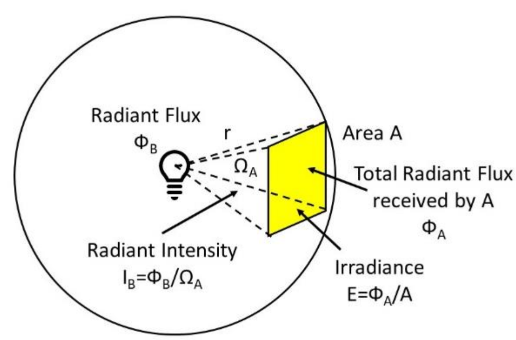

Figure 3. Schematics of optical radiation measurement quantities. The measurement plane (with area A) is normal to the bulb light source with subtended solid angle Ω_A. The total radiant flux emitted by the bulb is Φ_B. The radiant intensity, I_B, is therefore Φ_B/Ω_A and the total flux received by A, $\Phi_A=I_B\times\Omega_A$. The irradiance of A is therefore $E=\Phi_A/A$.

If we have the total radiant flux emitted by the source equally in all directions, Φ_B, and we divide it by the solid angle into which it radiates, a sphere or 4π in the above case, we may calculate the radiant intensity (I) in units of Watts per steradian. Understanding the radiant intensity, I, that a source emits in a particular direction and the solid angle, Ω, that a surface subtends to the source allows us to calculate the total energy received by the surface if it is perpendicular to it. In our example above,

$$\Phi_A = I_B \Omega \tag{3}$$

where I_B is the radiant intensity of the source. The area A has a finite area and receives total flux, Φ_A. We may calculate the Irradiance (E) as the radiant flux per unit area received by a surface orthogonal to the source. The irradiance at the measurement plane in Figure 3 is calculated as:

$$E = \frac{\Phi_A}{A} \tag{4}$$

and has units Watt per square meter.

Extended sources

Up to this point we have described a point source of light. In practice few sources of electromagnetic radiation are point sources and this should be accounted for in our measurements. Imagine that instead of a single point source we now have many point sources arranged next to each other all radiating in the same direction with the same radiant intensity, Figure 4. If the distance between the area A and the source is large enough that the solid angle between each of the point sources and the area is the same we could simple add up all of the point sources in a unit source area to yield the radiant flux falling on area A. Considering the extension of point sources in this manner we introduce term Radiance (L), or radiant flux per unit area per unit solid angle, with units of Watts per m^2 per sr.

In the example below, if the source has a radiance, L_S, of 5 $Wm^{-2}sr^{-1}$ and an area, A_S of $0.1m^2$ and the target an area of $0.25m^2$ and is 2 meters from the target, the radiant flux falling on the target is calculated as in the following manner. The solid angle of target is given by,

$$\Omega_T = \frac{0.25}{2^2} = \frac{0.25}{4} = \frac{1}{16} \text{ sr.} \tag{5}$$

The total flux falling on Target A is therefore calculated as,

$$\Phi_A = L_S A_s \Omega_T = 5 \times \frac{1}{10} \times \frac{1}{16} = \frac{1}{32} \text{ Watts.} \tag{6}$$

As the area of the target is $0.25m^2$, the irradiance is:

$$E = \frac{\Phi_A}{A} = \frac{1/32}{1/4} = \frac{1}{8} \text{ Wm}^{-2} \tag{7}$$

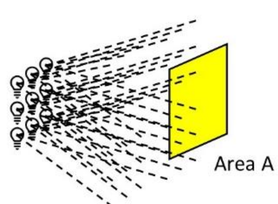

Figure 4. The extension of a single point source to many point sources illuminating a surface. Conceptually totaling the point source contributions per unit area of the source yields the radiance.

Spectral measurements and photometry

Total power emitted or received by a source or a surface has been discussed in the previous measurements. We could conduct all of these measurements for individual wavelengths of the electromagnetic spectrum. The radiant flux would become a graph of the energy in Watts per unit wavelength versus wavelength emitted by the source. The radiant intensity would become Watts per steradian per unit wavelength versus wavelength. Doing this we usually adopt the naming convention of spectral intensity, or spectral irradiance.

Measuring these types of quantities for each wavelength allows the scaling of results by the response of the human visual system, as mentioned previously, Figure 2, and thus allows for the estimation of the effect of sources on the human eye. These scaled responses yield equivalent photometric units for each of the radiometric units, Table 1. Photometry is important as it allows for the calculation of the perceived effect of sources on the human visual system. A Watt of light at 555nm at the peak sensitivity of the eye has a very different effect to that at 8 or 12μm in the far infra-red portion of the spectrum that we cannot see. Formally, the conversion from radiant flux to luminous flux, Φ_V, is expressed as [1, p102]:

$$\Phi_V = K_m \int \Phi(\lambda) \cdot V(\lambda)\, d\lambda \tag{8}$$

Where the subscript V generally denotes photometric quantities. V(λ) is the spectral luminous efficiency function or the normalized spectral sensitivity of averaged human eye. The unit of Φ_V is the lumen (lm) and K_m is the maximum luminous efficacy. K_m is 683 lm W^{-1} for photopic vision at 555nm and 1700 lm W^{-1} for scotopic vision at 510nm [2, p261]. Luminous intensity is the equivalent of radiant intensity and has the units of lumens per steradian, also known as candelas. Irradiance has the equivalent photometric equivalent of Illuminance and units of lumens per meter squared, also known as lux. Radiance is Luminance in its photometric form and has units of lumens per meter squared per steradian. Luminous intensity in candelas is usually used to define this and thus luminance usually takes the units of candelas per meter squared.

Table 1. Photometry and radiometry quantities

Quantity	Radiometry (SI unit)	Photometry (SI unit)
Power	Radiant flux (Watt, W)	Luminous flux (lumen, lm)
Power per solid angle	Radiant intensity (W sr^{-1})	Luminous intensity (candela=lm sr^{-1})
Power per unit area	Irradiance, radiant exitance (W m^{-2})	Illuminance, luminous exitance (lux = lm m^{-2})
Power per solid angle per unit area	Radiance (W m^{-2} sr^{-1})	Luminance (cd m^{-2})

Lambertian Surfaces

If reflected radiance is independent of viewing angle a surface is said to be Lambertian. That is, the Watts per steradian per square meter is approximately constant with respect to angle of viewing in radiometric units and likewise lumens per steradian per square meter in photometric units. This leads to the brightness of a Lambertian surface appearing approximately similar from all viewing angles. Matte white paper is a good approximation to a

Lambertian surface [1] as is the MacBeth Color Checker Classic chart. A simple relationship exists between the illuminance and luminance for Lambertian surfaces that make them particularly amenable to working with [3, p16]:

$$L_V = \frac{RE_V}{\pi}, \tag{9}$$

where R is reflectance, E_v, the illuminance and L_V, the luminance. Alternatively, the luminance is simply the lux falling on the surface multiplied by the reflectance and divided by π. For example, to estimate the luminance in cdm^{-2} coming from the 8% patch (Patch 23) of the MacBeth Color Checker Classic, it is simply,

$$L_V = \frac{0.08 \times E_V}{\pi}. \tag{10}$$

The inverse square law

Irradiance (or illuminance) from a point source is inversely proportional to the square of the distance from the source. This is the inverse square law. The decrease of irradiance with distance as $1/r^2$ can be shown as below. Substituting equation 4 into equation 3 we find,

$$E = \frac{I_B \Omega}{A} \tag{11}$$

and then equation 1 into 11,

$$E = \frac{I_B}{A} \cdot \frac{A}{r^2} = \frac{I_B}{r^2}\,. \tag{12}$$

The irradiance of a light falling onto a surface diminishes according to the square of the distance. It should also be noticed that they are no other terms in the denominator. Regardless of the radiant intensity or solid angle subtended by the source, it still obeys the inverse square law. Practically, high- or low-beam head lamps with narrow or wide beams will still diminish as the square of the distance.

Image Luminance Constancy

The inverse square law is often confused with principles governing the formation of images and it is often thought that the image luminance of objects decreases with increasing distance between the camera and the object. In the absence of atmospheric effects this is not the case and it may be shown that image luminance remains constant with distance. Richardson details an approachable description of the mathematics [4]. Figure 5 illustrates a camera of focal length, f, imaging an object at distance r. The apparent area of the pixel, A_P, projected into object space may be calculated using similar triangles as [4]:

$$A_P = x' . y' = \frac{x.y.r^2}{f^2} \tag{13}$$

where x and y are the dimension of the pixel and x', y' are the projected dimensions. The solid angle of the lens, Ω_L, of diameter, d, is [4]

$$\Omega_L = \frac{\pi d^2}{4r^2}. \tag{14}$$

If the luminance of the source is L_S, and the size of the source extends beyond the area of the projected pixel, the luminance in the pixel, L_P, is given by:

$$L_P = L_S A_P \Omega_L t_o t_a \tag{15}$$

where t_o and t_a are the transmission of the optics and atmosphere respectively. Substituting equations 13 and 14 into the above we find:

$$L_P = L_S . \frac{xyr^2}{f^2} . \frac{\pi d^2}{4r^2} t_o t_a \tag{16}$$

The r^2 terms are cancelled and we note that ${d^2}/{f^2}$ is the reciprocal of f-number, f#, yielding:

$$L_P = \frac{L_S xy \pi t_o t_a}{4 f\#^2}. \tag{17}$$

It may be seen in Equation 17 that there is no dependency on distance, r, aside from atmospheric attenuation, t_a. Thus, image luminance stays constant with distance in the absence of atmospheric effects. In practice, the amount of light imaged for the object does decrease with distance, but the size of the image of an object also decreases, keeping the image luminance constant with distance. It is worth emphasizing that this applies equally to self-luminous sources or reflected surfaces.

If for the question posed at the beginning of the paper you wrote different answers for 1(a) and 1(b) you may wish to reconsider.

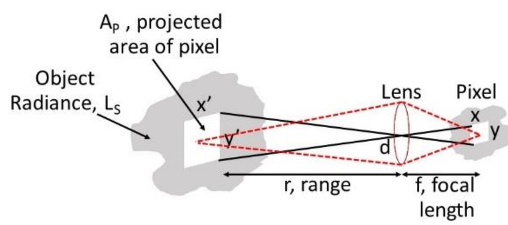

Figure 5, A simple model of a lens and pixel imaging a surface. Based on [4].

Illumination, Target, Lens, Sensor Model

The information given in the previous sections may be used to create an illumination - target – lens - sensor model that will give good first order approximations of the number of photoelectrons collected in pixel for given conditions from simple Lambertian reflectors orthogonal to the optical axis. The model is modified from that previously been detailed by Jenkin and Kane [5]. The desired ambient light level is first specified in lux, E_{AMB}, to scale a CIE D55 spectral curve, $W(\lambda)$, representing the illumination source [5]. The relative spectral luminous efficiency curve, $V(\lambda)$, of the CIE is scaled by the peak luminous efficacy of human vision (683 lumens per watt at 555 nm) [2, p261], multiplied by the D55 curve above and integrated to yield the total lux, $W(\lambda)$ represented by the illumination curve generated:

$$E_{SOURCE} = 683. \int_{\lambda_{MIN}}^{\lambda_{MAX}} W(\lambda) V(\lambda) d\lambda \tag{18}$$

where λ_{MAX} and λ_{MIN} are the maximum and minimum wavelengths of interest. E_{AMB} *is* divided by E_{SOURCE} to yield a multiplication factor, E_{SCALE}, by which to multiply $W(\lambda)$ so that it is correctly scaled to the wattage required to yield the lux desired in the scene.

The spectral reflectance curve of the target surface $S(\lambda)$ is multiplied by the scaled illumination curve and divided by π to give the spectral radiance of the surface in $Wm^{-2}sr^{-1}nm^{-1}$. Further multiplying by the absolute quantum efficiency curve of the sensor, $Q(\lambda)$, and absolute transmission of an infrared filter, $I(\lambda)$, yields the spectrum of light available to the sensor in $Wm^{-2}sr^{-1}nm^{-1}$ before lens and pixel geometry are considered, $P(\lambda)$, below.

$$P(\lambda) = \frac{E_{SCALE}}{\pi} W(\lambda) S(\lambda) I(\lambda) Q(\lambda) \quad (19)$$

In this model CIE D55 is used as the illumination spectra, shown in Figure 6 [2, p271]. The Macbeth Color Checker Classic patches are used as target spectra, Figure 7 [6]. Quantum efficiency curves are created by first modelling a typically monochrome curve peaking at approximately 83% and then multiplying that with those representing transmissions for red, green, blue, yellow, magenta and cyan color filter arrays, Figure 8 [7].

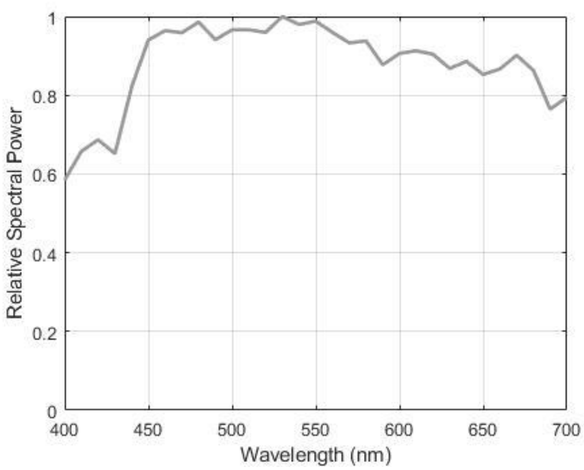

Figure 6, Relative Spectral Power of CIE D55 illumination [2, p271].

This intentionally does not represent any single sensor available at present but is a good approximation of current performance and quantum efficiency curves representing actual sensors may easily be substituted if necessary. The solid angle, Ω_L, of the lens collecting the signal reflected from the projected pixel area is calculated using equation 14. Multiplying by the solid angle and transmission of the lens, t_O, yields the power per nm per square meter, P_s, captured by the sensor:

$$P_s(\lambda) = \frac{E_{SCALE}}{\pi} W(\lambda) I(\lambda) Q(\lambda) \Omega_L t_o \quad (20)$$

A factor for losses due to windshield transmission may also be included in t_O. Multiplying by the area of the pixel, A_P, yields the power per nm per pixel, P_p.

$$P_p(\lambda) = \frac{E_{SCALE}}{\pi} W(\lambda) I(\lambda) Q(\lambda) \Omega_L t_o . A_p \quad (21)$$

The energy per photon, $\varepsilon(\lambda)$, is calculated using:

$$\varepsilon(\lambda) = \frac{hc}{\lambda} \quad (22)$$

where h is Plank's constant, 6.62x10-34 m^2 kg s^{-1}, and c is the speed of light, 299792458 ms^{-1}. Dividing $P_p(\lambda)$ by $\varepsilon(\lambda)$, multiplying by the integration time, T_{INT}, and integrating yields the total number of photoelectrons captured by the pixel, PE_p:

$$PE_p = \int_{\lambda_{MIN}}^{\lambda_{MAX}} \frac{T_{INT} . P_p(\lambda)}{\varepsilon(\lambda)} d\lambda \quad (23)$$

The above model represents a relatively simple single exposure regime. By repeating calculations with different exposure times or adding an attenuation term, it is relatively simple to extend the model to estimate photoelectrons collected for sequential or other high dynamic range exposure (HDR) schemes.

It should also be noted that the surface modeling here only accounts for diffusely lit Lambertian patches orthogonal to the optical axis of the camera. Specular and retroreflective materials with different lighting geometries will yield different results.

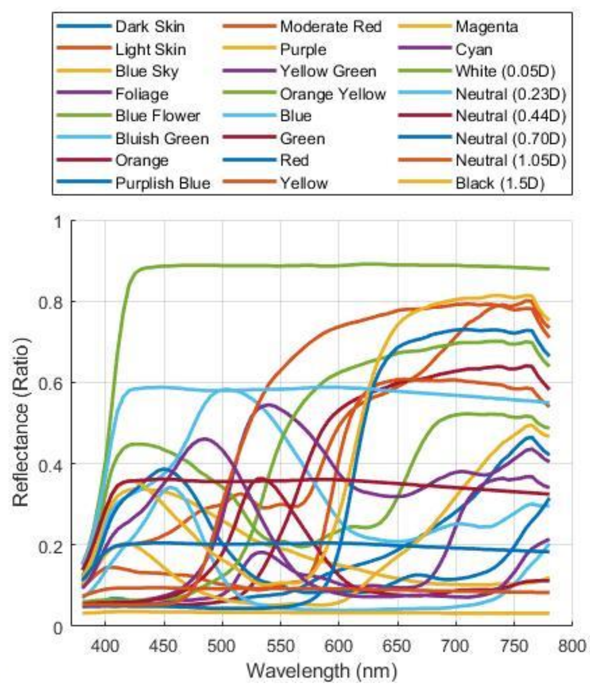

Figure 7, Spectral reflectance of the MacBeth Color Checker Classic patches [6].

Imaging Performance for typical parameters

Using the above model, it is possible to estimate photoelectrons per lux-second at the sensor plane for D55 daylight and the MacBeth color chart for a variety of conditions, pixel sizes and CFA filters, Table 2. Calculated for an f1.4 lens, the first row, "Geo", represents the photons available if only the geometry of the imaging is considered between 400 and 700nm. The aperture f1.4 is chosen as it represents the leading edge of what is available in automotive manufacturing at present. No losses due to lens transmission, IRCF, windshield or quantum efficiency are added. This represents the maximum amount of light available to the sensor for conversion into signal and gives a fundamental envelope of performance in this wavelength range.

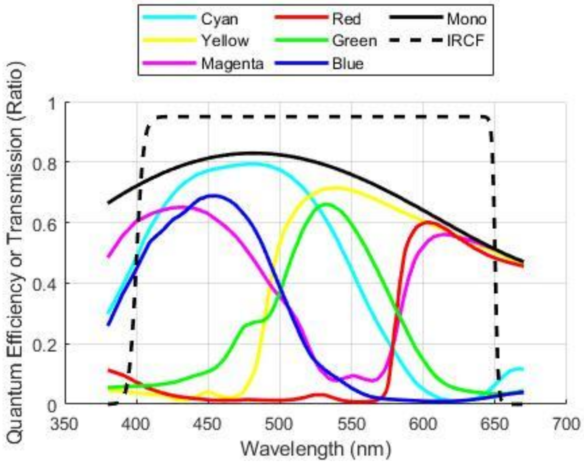

Figure 8, Quantum efficiency curves of each of the color channels created using data for CFA filter materials [7]. Also shown is the IRCF transmission curve used.

If the data for Patch 22 is examined, we can see that approximately 1000 photons are generated per lux-second for a 2µm pixel with D55 at f1.4. The reflectance of the patch is approximately 18.7% between 400 and 700nm [6]. Using this as a starting point we can create a mental model to estimate the photons available to a sensor for other conditions. Rounding the reflectance of patch 22 to 20% we can state "*Patch 22 (20%) for 2µm at f√2 gives 1 photon per lux per ms".* This can then be modified to yield other results. A stop in any direction will double or halve the result. e.g f2 will give 0.5 photons per lux per ms. Photons will be proportional to pixel area. Doubling the pixel size will yield four times the number of photons. For automotive purposes it is then possible to add in degradation to account for lens transmission (0.95), IRCF transmission (0.95 between 400 and 650nm), windshield losses (0.7) and the color filter array. For a monochrome array the available signal is approximately 0.4x when the above losses and silicon sensitivity are factored in. For RGB CFAs this drops to between 0.1x (Red) and 0.15x (Green) and for CMY CFAs 0.2x (Magenta) to 0.25x (Yellow). Finally, for 2.1µm pixels, as this is a common node, we can add 10%.

While far from perfect, this approach gives engineers a starting point with which to estimate the order of magnitude of a signal available from a pixel. Using our car example, Figure 1(a) which calls for estimating the signal from 10lux daylight using an f1.4 lens and 2.1μm pixel with a 10ms exposure in clear conditions with no losses from a 20% reflective surface. We start with the mental model "20% f√2 (f1.4) at with a 2µm pixel gives 1 photon per ms". For 10ms at 10 lux this would yield 100 photons. Add 10% to uprate to a 2.1µm pixel modifies our estimate to 110 photons. If we wanted to estimate signal in the green channel after losses, we further multiply by 0.15 = 16 photons. Performing the actual calculation with the model yields 119 and 17 photons. The estimate is well within an order of magnitude of the actual result.

Further examining Table 2, we observe that imaged photons are somewhere between 10% and 25% of the available photons once losses due to the lens, windshield, IRCF and quantum efficiency are accounted for. While losses in any one process may appear manageable, it is worth remembering that they are multiplicative and quickly collapse the available signal envelope. It is also worth noting that the effective sensitivity of the system is a fraction of the 10's of thousands of electrons per lux-second for sensitivity usually quoted by sensor manufacturers. This is because sensitivity measurements are often made by directly illuminating the sensor and do not account for lens geometries, surface reflectance or other system losses.

Signal variance due to the quantized nature of light, or shot noise as it is known, is equal to the number of quanta present. Therefore, using RMS fluctuations (the square root of the number of quanta) to calculate signal-to-noise ratio due to shot noise, we find it is directly proportional to the size of the pixel. Total SNR, however, includes a fixed noise component of a few electrons, consisting of a number of contributors, such a read noise, dark signal non-uniformity and dark current. As these components are signal independent and generally increase with temperature, they quickly dominate signal-to-noise performance at low light levels.

Table 3 shows photoelectrons for a D55 5lux 10ms exposure with a f1.4 aperture. If we wish to achieve a linear SNR of 1 and the fixed noise component is a total of 3 electrons RMS at least 3.5 photoelectrons of signal are required. For a linear SNR of 4, in excess 22.4 photoelectrons are needed. Examining Table 3 we can see that at 5 lux, all but the brightest Macbeth patches at the 2.1µm node with a CFA applied struggle to achieve the desired number of photoelectrons for an SNR of 4. We conclude, that for the modelled system, below 5 lux we will rapidly approach the noise floor of the sensor and should expect the system performance to degrade significantly.

Summary

A primer of basic radiometry and photometry was outlined and used to construct an elementary model of an illumination source, Lambertian surface, lens and sensor with the intention of giving engineers new to the field or those already working with cameras an introduction to the subject. The imaging model was used to illustrate how it is possible to establish fundamental performance limits for an imaging system. A mental model was also offered that can yield first order approximations of photoelectrons in pixel for typical quantum efficiencies and system losses available at present.

References

[1] R. W. Boyd, Radiometry and the Detection of Optical Radiation, Rochester, New York: John Wiley and Sons Inc., 1982.

[2] R. W. G. Hunt, Measuring Color, 2nd Ed., London: Ellis Horwood Limited, 1995.

[3] M. A. Richardson et al, Surveillance and Target Acquisition Systems, 2nd Ed., London: Brassey's (UK) Limited, 1997.

[4] M. A. Richardson, "Electro-Optical Systems Analysis Part 2" Journal Battlefield Technol., vol. 5, no. 3, p. 21, 2002.

[5] R. Jenkin and P. Kane, "Fundamental Imaging System Analysis for Autonomous Vehicles", Proc. IS&T Electronic Imaging, Autonomous Vehicles and Machines 2018, Burlingame, California, 2018.

[6] BabelColor, https://www.babelcolor.com/colorchecker.htm, Last accessed June 2021.

[7] Fuji Film (United States) Corporation, https://www.fujifilm.com/us/en/business/semiconductor-

materials/image-sensor-color-mosaic/cmy/applications, Last accessed June 2021.

Author Biographies

Robin Jenkin received, BSc(Hons) Photographic and Electronic Imaging Science (1995) and his PhD (2001) in the field of image science from University of Westminster. He also holds a M.Res Computer Vision and Image Processing from University College London (1996). Robin is a Fellow of The Royal Photographic Society, UK, and a board member and VP Publications of IS&T. Robin works at NVIDIA Corporation where he models image quality for autonomous vehicle applications. He is a Visiting Professor at University of Westminster within the Computer Vision and Imaging Technology Research Group.

Cheng Zhao received MSc(2007) and PhD(2013) in the field of Optoelectronics from University of Rochester. She works at NVIDIA Corporation on image quality modeling for autonomous vehicle applications, with the focus on the impacts of camera optical performance. Previously, she worked for OmniVision Technologies, Inc where she did optical modeling for CMOS image sensors.

Table 2. Photoelectrons per lux-second for a f1.4 lens imaging diffusely lit MacBeth Color Checker patches with CIE D55 illumination.

Patch Number 1 - Dark Skin

Px Sz	1	2	2.1	2.25	3
Geo	164	658	725	833	1480
Mono	45	178	196	225	401
Red	19	75	83	95	169
Grn	16	62	69	79	141
Ble	10	39	43	49	88
Cyn	20	79	87	100	178
Mgn	27	107	118	135	240
Ylw	33	133	147	169	300

Patch Number 2 - Light Skin

Px Sz	1	2	2.1	2.25	3
Geo	553	2213	2439	2800	4978
Mono	168	673	742	852	1515
Red	65	260	286	329	584
Grn	61	244	269	308	548
Ble	42	167	184	211	376
Cyn	83	330	364	418	743
Mgn	99	396	436	501	890
Ylw	122	486	536	616	1095

Patch Number 3 - Blue Sky

Px Sz	1	2	2.1	2.25	3
Geo	263	1053	1161	1333	2369
Mono	111	445	490	563	1001
Red	19	77	85	97	173
Grn	41	165	182	209	372
Ble	48	190	210	241	428
Cyn	78	312	344	395	702
Mgn	61	245	271	311	552
Ylw	57	228	251	289	513

Patch Number 4 - Foliage

Px Sz	1	2	2.1	2.25	3
Geo	147	586	646	742	1319
Mono	51	204	225	258	459
Red	13	53	58	67	119
Grn	24	97	107	123	218
Ble	12	47	52	60	106
Cyn	29	114	126	145	257
Mgn	23	93	102	117	209
Ylw	38	153	169	194	344

Patch Number 5 - Blue Flower

Px Sz	1	2	2.1	2.25	3
Geo	437	1749	1928	2214	3936
Mono	148	593	654	751	1335
Red	32	130	143	165	292
Grn	51	204	224	258	458
Ble	62	248	274	314	559
Cyn	99	397	438	503	894
Mgn	87	349	384	441	785
Ylw	77	310	341	392	697

Patch Number 6 - Bluish Green

Px Sz	1	2	2.1	2.25	3
Geo	484	1935	2134	2449	4354
Mono	201	805	888	1019	1812
Red	33	133	147	169	300
Grn	90	361	398	457	812
Ble	71	284	313	360	639
Cyn	138	551	607	697	1239
Mgn	95	381	420	482	857
Ylw	124	495	546	627	1114

Patch Number 7 - Orange

Px Sz	1	2	2.1	2.25	3
Geo	451	1803	1988	2282	4056
Mono	119	476	524	602	1070
Red	67	270	297	341	606
Grn	39	158	174	200	355
Ble	12	47	52	60	106
Cyn	34	135	148	170	303
Mgn	74	298	328	377	670
Ylw	104	418	460	529	940

Patch Number 8 - Purplish Blue

Px Sz	1	2	2.1	2.25	3
Geo	219	877	967	1110	1974
Mono	90	361	398	457	812
Red	13	51	56	64	114
Grn	29	114	126	144	257
Ble	47	189	209	239	426
Cyn	69	276	304	349	621
Mgn	55	219	241	277	493
Ylw	36	143	157	180	321

Patch Number 9 - Moderate Red

Px Sz	1	2	2.1	2.25	3
Geo	411	1646	1814	2083	3703
Mono	104	414	457	524	932
Red	59	237	261	299	532
Grn	27	106	117	134	239
Ble	21	83	91	105	186
Cyn	36	145	160	184	326
Mgn	75	300	331	380	675
Ylw	79	317	350	402	714

Patch Number 10 - Purple

Px Sz	1	2	2.1	2.25	3
Geo	163	653	720	826	1469
Mono	45	182	200	230	409
Red	12	50	55	63	111
Grn	13	52	57	65	116
Ble	19	77	85	97	173
Cyn	28	114	125	144	256
Mgn	30	119	132	151	269
Ylw	23	92	101	116	206

Patch Number 11 - Yellow Green

Px Sz	1	2	2.1	2.25	3
Geo	438	1752	1932	2218	3943
Mono	156	626	690	792	1408
Red	45	182	200	230	409
Grn	78	313	345	397	705
Ble	27	106	117	134	239
Cyn	80	320	353	405	720
Mgn	67	268	295	339	603
Ylw	129	516	569	654	1162

Patch Number 12 - Orange Yellow

Px Sz	1	2	2.1	2.25	3
Geo	569	2277	2510	2882	5123
Mono	164	658	725	832	1479
Red	79	314	347	398	707
Grn	64	257	283	325	577
Ble	18	74	82	94	166
Cyn	57	227	251	288	512
Mgn	91	365	402	462	821
Ylw	143	572	630	724	1287

Patch Number 13 - Blue

Px Sz	1	2	2.1	2.25	3
Geo	134	537	592	679	1207
Mono	60	240	265	304	540
Red	6	25	27	31	55
Grn	17	68	75	87	154
Ble	36	144	159	182	324
Cyn	49	196	217	249	442
Mgn	38	152	168	192	342
Ylw	18	73	80	92	164

Patch Number 14 - Green

Px Sz	1	2	2.1	2.25	3
Geo	202	807	890	1021	1816
Mono	85	341	376	431	766
Red	15	59	65	75	133
Grn	47	186	205	236	419
Ble	20	78	86	99	176
Cyn	53	211	233	267	475
Mgn	32	127	140	161	285
Ylw	65	260	287	329	586

Patch Number 15 - Red

Px Sz	1	2	2.1	2.25	3
Geo	361	1446	1594	1830	3253
Mono	68	270	298	342	608
Red	48	191	210	241	429
Grn	14	55	61	70	124
Ble	9	35	39	44	79
Cyn	16	64	71	81	144
Mgn	54	217	239	275	488
Ylw	57	230	253	291	517

Patch Number 16 - Yellow

Px Sz	1	2	2.1	2.25	3
Geo	719	2875	3169	3638	6468
Mono	221	883	974	1118	1987
Red	93	372	410	470	836
Grn	96	384	423	486	863
Ble	27	108	119	137	243
Cyn	89	354	391	448	797
Mgn	112	450	496	569	1012
Ylw	192	769	848	974	1731

Patch Number 17 - Magenta

Px Sz	1	2	2.1	2.25	3
Geo	504	2016	2223	2552	4537
Mono	127	508	560	643	1144
Red	56	224	247	284	505
Grn	31	126	139	159	283
Ble	41	162	179	206	365
Cyn	61	245	270	310	551
Mgn	91	366	403	463	823
Ylw	80	319	351	403	717

Patch Number 18 - Cyan

Px Sz	1	2	2.1	2.25	3
Geo	267	1067	1177	1351	2401
Mono	121	485	535	614	1091
Red	12	48	53	60	107
Grn	49	196	216	248	441
Ble	58	230	254	291	518
Cyn	96	384	424	487	865
Mgn	62	250	276	316	562
Ylw	58	231	254	292	519

Patch Number 19 - White (0.05D)

Px Sz	1	2	2.1	2.25	3
Geo	1181	4726	5210	5981	10633
Mono	434	1735	1913	2196	3903
Red	115	458	505	580	1031
Grn	169	678	747	858	1525
Ble	140	558	616	707	1256
Cyn	258	1034	1140	1308	2326
Mgn	234	938	1034	1187	2110
Ylw	277	1107	1221	1401	2491

Patch Number 20 - Neutral (0.23D)

Px Sz	1	2	2.1	2.25	3
Geo	778	3114	3433	3941	7006
Mono	287	1148	1266	1454	2584
Red	76	302	333	382	680
Grn	112	446	492	565	1004
Ble	93	373	411	472	838
Cyn	171	685	756	867	1542
Mgn	156	623	687	789	1402
Ylw	182	728	803	922	1639

Patch Number 21 - Neutral (0.44D)

Px Sz	1	2	2.1	2.25	3
Geo	477	1909	2104	2416	4294
Mono	177	706	779	894	1589
Red	46	185	204	234	416
Grn	69	274	302	347	617
Ble	58	230	254	291	518
Cyn	106	422	466	534	950
Mgn	96	383	423	485	863
Ylw	112	446	492	565	1004

Patch Number 22 - Neutral (0.70D)

Px Sz	1	2	2.1	2.25	3
Geo	271	1082	1193	1370	2435
Mono	100	401	442	507	902
Red	26	105	116	133	236
Grn	39	155	171	197	350
Ble	33	131	144	165	294
Cyn	60	240	264	303	539
Mgn	54	218	240	276	490
Ylw	63	253	279	320	570

Patch Number 23 - Neutral (1.05D)

Px Sz	1	2	2.1	2.25	3
Geo	123	493	544	624	1109
Mono	46	183	202	232	413
Red	12	47	52	60	106
Grn	18	71	78	90	160
Ble	15	60	67	76	136
Cyn	28	110	122	140	248
Mgn	25	100	110	126	224
Ylw	29	115	127	146	259

Patch Number 24 - Black (1.5D)

Px Sz	1	2	2.1	2.25	3
Geo	45	181	200	229	407
Mono	17	67	74	85	151
Red	4	17	19	22	39
Grn	6	26	29	33	58
Ble	6	22	25	28	50
Cyn	10	41	45	51	92
Mgn	9	37	40	46	82
Ylw	10	42	46	53	94

Table 3. Photoelectrons per lux-second for a f1.4 lens imaging diffusely lit MacBeth Color Checker patches with CIE D55 illumination at 5 lux for an exposure time of 10ms.

Patch Number 1 - Dark Skin

Px Sz	1	2	2.1	2.25	3
Geo	8	33	36	42	74
Mono	2	9	10	11	20
Red	1	4	4	5	8
Grn	1	3	3	4	7
Ble	0	2	2	2	4
Cyn	1	4	4	5	9
Mgn	1	5	6	7	12
Ylw	2	7	7	8	15

Patch Number 2 - Light Skin

Px Sz	1	2	2.1	2.25	3
Geo	28	111	122	140	249
Mono	8	34	37	43	76
Red	3	13	14	16	29
Grn	3	12	13	15	27
Ble	2	8	9	11	19
Cyn	4	17	18	21	37
Mgn	5	20	22	25	45
Ylw	6	24	27	31	55

Patch Number 3 - Blue Sky

Px Sz	1	2	2.1	2.25	3
Geo	13	53	58	67	118
Mono	6	22	25	28	50
Red	1	4	4	5	9
Grn	2	8	9	10	19
Ble	2	10	10	12	21
Cyn	4	16	17	20	35
Mgn	3	12	14	16	28
Ylw	3	11	13	14	26

Patch Number 4 - Foliage

Px Sz	1	2	2.1	2.25	3
Geo	7	29	32	37	66
Mono	3	10	11	13	23
Red	1	3	3	3	6
Grn	1	5	5	6	11
Ble	1	2	3	3	5
Cyn	1	6	6	7	13
Mgn	1	5	5	6	10
Ylw	2	8	8	10	17

Patch Number 5 - Blue Flower

Px Sz	1	2	2.1	2.25	3
Geo	22	87	96	111	197
Mono	7	30	33	38	67
Red	2	6	7	8	15
Grn	3	10	11	13	23
Ble	3	12	14	16	28
Cyn	5	20	22	25	45
Mgn	4	17	19	22	39
Ylw	4	15	17	20	35

Patch Number 6 - Bluish Green

Px Sz	1	2	2.1	2.25	3
Geo	24	97	107	122	218
Mono	10	40	44	51	91
Red	2	7	7	8	15
Grn	5	18	20	23	41
Ble	4	14	16	18	32
Cyn	7	28	30	35	62
Mgn	5	19	21	24	43
Ylw	6	25	27	31	56

Patch Number 7 - Orange

Px Sz	1	2	2.1	2.25	3
Geo	23	90	99	114	203
Mono	6	24	26	30	54
Red	3	13	15	17	30
Grn	2	8	9	10	18
Ble	1	2	3	3	5
Cyn	2	7	7	9	15
Mgn	4	15	16	19	33
Ylw	5	21	23	26	47

Patch Number 8 - Purplish Blue

Px Sz	1	2	2.1	2.25	3
Geo	11	44	48	56	99
Mono	5	18	20	23	41
Red	1	3	3	3	6
Grn	1	6	6	7	13
Ble	2	9	10	12	21
Cyn	3	14	15	17	31
Mgn	3	11	12	14	25
Ylw	2	7	8	9	16

Patch Number 9 - Moderate Red

Px Sz	1	2	2.1	2.25	3
Geo	21	82	91	104	185
Mono	5	21	23	26	47
Red	3	12	13	15	27
Grn	1	5	6	7	12
Ble	1	4	5	5	9
Cyn	2	7	8	9	16
Mgn	4	15	17	19	34
Ylw	4	16	17	20	36

Patch Number 10 - Purple

Px Sz	1	2	2.1	2.25	3
Geo	8	33	36	41	73
Mono	2	9	10	11	20
Red	1	2	3	3	6
Grn	1	3	3	3	6
Ble	1	4	4	5	9
Cyn	1	6	6	7	13
Mgn	1	6	7	8	13
Ylw	1	5	5	6	10

Patch Number 11 - Yellow Green

Px Sz	1	2	2.1	2.25	3
Geo	22	88	97	111	197
Mono	8	31	34	40	70
Red	2	9	10	11	20
Grn	4	16	17	20	35
Ble	1	5	6	7	12
Cyn	4	16	18	20	36
Mgn	3	13	15	17	30
Ylw	6	26	28	33	58

Patch Number 12 - Orange Yellow

Px Sz	1	2	2.1	2.25	3
Geo	28	114	126	144	256
Mono	8	33	36	42	74
Red	4	16	17	20	35
Grn	3	13	14	16	29
Ble	1	4	4	5	8
Cyn	3	11	13	14	26
Mgn	5	18	20	23	41
Ylw	7	29	32	36	64

Patch Number 13 - Blue

Px Sz	1	2	2.1	2.25	3
Geo	7	27	30	34	60
Mono	3	12	13	15	27
Red	0	1	1	2	3
Grn	1	3	4	4	8
Ble	2	7	8	9	16
Cyn	2	10	11	12	22
Mgn	2	8	8	10	17
Ylw	1	4	4	5	8

Patch Number 14 - Green

Px Sz	1	2	2.1	2.25	3
Geo	10	40	44	51	91
Mono	4	17	19	22	38
Red	1	3	3	4	7
Grn	2	9	10	12	21
Ble	1	4	4	5	9
Cyn	3	11	12	13	24
Mgn	2	6	7	8	14
Ylw	3	13	14	16	29

Patch Number 15 - Red

Px Sz	1	2	2.1	2.25	3
Geo	18	72	80	91	163
Mono	3	14	15	17	30
Red	2	10	11	12	21
Grn	1	3	3	3	6
Ble	0	2	2	2	4
Cyn	1	3	4	4	7
Mgn	3	11	12	14	24
Ylw	3	11	13	15	26

Patch Number 16 - Yellow

Px Sz	1	2	2.1	2.25	3
Geo	36	144	158	182	323
Mono	11	44	49	56	99
Red	5	19	20	24	42
Grn	5	19	21	24	43
Ble	1	5	6	7	12
Cyn	4	18	20	22	40
Mgn	6	22	25	28	51
Ylw	10	38	42	49	87

Patch Number 17 - Magenta

Px Sz	1	2	2.1	2.25	3
Geo	25	101	111	128	227
Mono	6	25	28	32	57
Red	3	11	12	14	25
Grn	2	6	7	8	14
Ble	2	8	9	10	18
Cyn	3	12	14	16	28
Mgn	5	18	20	23	41
Ylw	4	16	18	20	36

Patch Number 18 - Cyan

Px Sz	1	2	2.1	2.25	3
Geo	13	53	59	68	120
Mono	6	24	27	31	55
Red	1	2	3	3	5
Grn	2	10	11	12	22
Ble	3	12	13	15	26
Cyn	5	19	21	24	43
Mgn	3	12	14	16	28
Ylw	3	12	13	15	26

Patch Number 19 - White (0.05D)

Px Sz	1	2	2.1	2.25	3
Geo	59	236	261	299	532
Mono	22	87	96	110	195
Red	6	23	25	29	52
Grn	8	34	37	43	76
Ble	7	28	31	35	63
Cyn	13	52	57	65	116
Mgn	12	47	52	59	105
Ylw	14	55	61	70	125

Patch Number 20 - Neutral (0.23D)

Px Sz	1	2	2.1	2.25	3
Geo	39	156	172	197	350
Mono	14	57	63	73	129
Red	4	15	17	19	34
Grn	6	22	25	28	50
Ble	5	19	21	24	42
Cyn	9	34	38	43	77
Mgn	8	31	34	39	70
Ylw	9	36	40	46	82

Patch Number 21 - Neutral (0.44D)

Px Sz	1	2	2.1	2.25	3
Geo	24	95	105	121	215
Mono	9	35	39	45	79
Red	2	9	10	12	21
Grn	3	14	15	17	31
Ble	3	12	13	15	26
Cyn	5	21	23	27	48
Mgn	5	19	21	24	43
Ylw	6	22	25	28	50

Patch Number 22 - Neutral (0.70D)

Px Sz	1	2	2.1	2.25	3
Geo	14	54	60	68	122
Mono	5	20	22	25	45
Red	1	5	6	7	12
Grn	2	8	9	10	17
Ble	2	7	7	8	15
Cyn	3	12	13	15	27
Mgn	3	11	12	14	24
Ylw	3	13	14	16	28

Patch Number 23 - Neutral (1.05D)

Px Sz	1	2	2.1	2.25	3
Geo	6	25	27	31	55
Mono	2	9	10	12	21
Red	1	2	3	3	5
Grn	1	4	4	5	8
Ble	1	3	3	4	7
Cyn	1	6	6	7	12
Mgn	1	5	5	6	11
Ylw	1	6	6	7	13

Patch Number 24 - Black (1.5D)

Px Sz	1	2	2.1	2.25	3
Geo	2	9	10	11	20
Mono	1	3	4	4	8
Red	0	1	1	1	2
Grn	0	1	1	2	3
Ble	0	1	1	1	3
Cyn	1	2	2	3	5
Mgn	0	2	2	2	4
Ylw	1	2	2	3	5